Experimental Neurology 351 (2022) 114010

Contents lists available at ScienceDirect

Experimental Neurology

journal homepage: www.elsevier.com/locate/yexnr

Research paper

Cisplatin toxicity in the developing brain displays an absolute requirement for caspase-3

Kelvin K. Hui [a,b,c,1], Maya Latif [a,1], Chesa Dojo Soeandy [a], Shudi Huang [a], Christopher E. Rodgers [a], Andrew J. Elia [d,e], Jeffrey T. Henderson [a,*]

[a] Graduate Department of Pharmaceutical Sciences, University of Toronto, Toronto, Ontario, Canada
[b] Department of Developmental and Molecular Biology, Albert Einstein College of Medicine, Bronx, New York, USA
[c] Institute for Aging Studies, Albert Einstein College of Medicine, Bronx, New York, USA
[d] Princess Margaret Cancer Center, University Health Network, Toronto, Ontario, Canada
[e] Department of Medical Biophysics, University of Toronto, Toronto, Ontario, Canada

ARTICLE INFO

Keywords:
Apoptosis
Caspases
Cisplatin
Neural stem cells

ABSTRACT

Cisplatin is a member of a widely utilized class of chemotherapeutic agent that initiates DNA damage response, cell cycle arrest, and p53-dependent apoptotic cell death in concert with DNA-platinum adduct formation. While normal programmed cell death (PCD) can occur in the developing neuroepithelium in the absence of caspase-3 within certain genetic backgrounds, we observed an absolute dependency upon this executioner caspase with respect to cisplatin-induced PCD in the developing central nervous system (CNS). We therefore examined the nature of this genotoxic injury in the CNS *in vivo,* in which cisplatin treatment causes widespread cellular injury consistent with hallmarks of apoptosis which are averted upon caspase-3 inhibition. Examination of cisplatin-mediated injury as a function of time revealed the presence of an alternative, delayed form of necroptosis-like cell death which manifests in *Casp3*$^{-/-}$ neuroepithelia for several days following the normal pattern of apoptosis. Together, these findings suggest a coordinated regulation of these disparate PCD pathways in response to genotoxic stress *in vivo* and highlight the unique and critical role which caspase-3 plays among executioner caspases in coordinating apoptotic *versus* necroptotic responsiveness of the developing CNS to genotoxic injury.

1. Introduction

Platinum-based chemotherapeutic agents, including the parent compound cis-diamminedichloridoplatinum (II) commonly known as cisplatin, are effective in treating a variety of solid tumours including malignant glioblastoma, head and neck, gastric, cervical, ovarian, and testicular cancers (Dasari and Tchounwou, 2014). Usage of such platinum-based agents however is limited by significant side effects including neuro- and ototoxicity in addition to kidney damage. With respect to the CNS, a condition known as “chemo brain” has been observed in which cognitive impairment, changes to white matter, encephalopathy, seizures, and strokes in conjunction with peripheral neuropathy have all been described in association with cisplatin treatment (Minisini et al., 2004). Observed central CNS effects have been attributed to significant concentrations of drug which can be attained in the brain where it exhibits toxicity toward proliferating neural precursor and neural stem cells (Dietrich et al., 2006).

The principal mechanism of cytotoxicity for cisplatin and related compounds is thought to occur through activation of p53 genotoxic surveillance systems in conjunction with formation of DNA adducts ultimately resulting in DNA double-stranded breaks; interfering with DNA replication and cell proliferation (Dasari and Tchounwou, 2014). Such lesions are in turn recognized by ATM and ATR which activate DNA damage response systems and inhibit cell cycle progression *via* regulators such as p53, p21, Chk1, and Chk2 (Awasthi et al., 2015). In addition to blocking cell cycle progression, p53 signalling also acts to transcriptionally upregulate proapoptotic genes such as Puma and Bax, thus promoting mitochondrial outer membrane permeabilization (MOMP) (Nakano and Vousden, 2001; Toshiyuki and Reed, 1995). This in turn triggers release of cytochrome *c* and apoptosis inducing factor (AIF)

* Corresponding author at: Graduate Department of Pharmaceutical Sciences, Faculty of Pharmacy, University of Toronto, 144 College Street, Room 903, Toronto, Ontario M5S 3M2, Canada.
E-mail address: jeff.henderson@utoronto.ca (J.T. Henderson).
[1] These authors contributed equally to this paper.

https://doi.org/10.1016/j.expneurol.2022.114010
Received 27 January 2021; Received in revised form 26 January 2022; Accepted 8 February 2022
Available online 12 February 2022

from the mitochondria, initiating caspase-dependent and caspase-independent signalling responsible for promoting the irreversible phase of cell death (Singh et al., 2019). Interestingly, reductions in cellular activation of caspase-3 have been observed in renal cells and several oncogenic models correlated with enhanced cisplatin resistance (Blanc et al., 2000; Kamarajan et al., 2001; Yang et al., 2004). Consistent with this, a variety of normal and cancer cell lines have demonstrated cisplatin-induced cell death to be both delayed and reduced upon depletion of caspase-3 (Cummings and Schnellmann, 2002). However there are also reports of elevated caspase-3 activation in cisplatin-resistant ovarian cancer cell lines compared to cisplatin-sensitive ones (Henkels and Turchi, 1999). Thus, the exact role of caspase-3 in mediating cisplatin-induced cell death *in vivo*, particularly in the CNS, has yet to be carefully examined.

Previously, we and others have examined the role of caspase-3 in regulating development of the murine CNS (Kanungo et al., 2009; Kuida et al., 1996; Woo et al., 1998). These studies demonstrated that in certain genetic backgrounds the loss of caspase-3 resulted in overgrowth in neural populations in the CNS (similar in nature and extent to alterations subsequently seen following ablation of caspase-9 or Apaf-1 (Cecconi et al., 1998; Hakem et al., 1998; Kuida et al., 1998; Yoshida et al., 1998)), thereby identifying the key role of this executioner caspase in regulating PCD in the developing CNS. Subsequent to these studies, genetic backgrounds such as C57BL/6 J were identified in which the loss of caspase-3 does not cause disruption of murine CNS development, resulting in mice with normal lifespan and fecundity, which has been suggested to be due to an increase in compensatory executioner caspases in this background (Houde et al., 2004). In order to better understand the true role of caspase-3 in mediating cisplatin-induced toxicity in this tissue, we have utilized this genetic background and that of others to examine its effects in regulating PCD. Surprisingly, we observe that even within the C57BL/6 J background, cisplatin-induced PCD exhibits a striking dependence upon the activity of caspase-3.

Specifically, within this study we investigated the *in vivo* requirement for capase-3 in cisplatin-induced cell death in the developing neuroepithelium, observing that its absence did not affect upstream cell PCD signalling. However, contrary to findings seen for naturally occurring programmed cell death, our observations reveal an absolute requirement for caspase-3 in cisplatin-mediated programmed cell death within the developing brain. Our findings further indicate that necroptotic PCD is not normally activated in the presence of caspase-3 during cisplatin treatment, nor is it immediately initiated in the absence of caspase-3; but rather occurs in a delayed and limited manner several days following cisplatin treatment in the absence of caspase-3. These findings indicate that apoptosis is the predominant programmed cell death pathway initiated by cisplatin treatment in the developing neuroepithelia, with necroptosis serving only as a secondary pathway in a minor subpopulation of cells unable to withstand cisplatin toxicity.

2. Results

2.1. Ablation of Caspase-3 completely abolishes cisplatin-induced apoptotic cell death

In order to examine the effects of cisplatin-induced DNA damage in the developing brain, pregnant dams were treated with 10 or 20 mg/kg of cisplatin on embryonic day 12.5 (E12.5) (Köpf-Maier and Merker, 1983). *Casp3*$^{+/+}$ (WT), *Casp3*$^{+/-}$ (heterozygous), and *Casp3*$^{-/-}$ (null) embryos were initially collected at 24 h following cisplatin or control vehicle treatment and examined for their patterns of cell death. Similar to previous reports revealing that *Casp3* null animals on a C57BL/6 J background undergo normal development with no detectable defects in brain formation (Houde et al., 2004; Hui et al., 2011; Woo et al., 1998), no significant genotype differences in cell number in different regions of the developing brain were observed following vehicle treatment (Supplementary Fig. 1A). By contrast, substantial cell death was observed in the germinal and early neuroepithelial layers of the developing neocortex, developing striatum, the cephalic flexure of the midbrain, and the thalamic nuclei in response to cisplatin treatment in *Casp3*$^{+/+}$ and *Casp3*$^{+/-}$ embryos. Strikingly, there were no such signs of cell death in any of these regions in *Casp3* null littermate embryos (Fig. 1A-B, Supplementary Fig. 1B-C), suggesting a differential requirement for caspase-3 in cisplatin-induced PCD (Houde et al., 2004; Woo et al., 1998).

Given the known role of caspase-3 in regulating apoptotic PCD, we examined the time course of apoptotic cell death occurring in wild-type (WT) embryos collected at different time points following cisplatin treatment. As shown in Supplementary Fig. 2, apoptotic cell death, as measured by both caspase-3 activation and terminal deoxynucleotidyl transferase dUTP nick end labeling (TUNEL) staining, begins to rise at 12 h post-treatment, becomes maximal at 24–48 h following treatment and returns to baseline by 72 h post-cisplatin treatment. Based upon this, we continued our analysis over this time frame and observed surprisingly a near total absence of TUNEL^{+} cells in *Casp3* null embryos (Fig. 1C-D), as both WT and *Casp3* heterozygote embryos displayed significant increases in TUNEL^{+} cells (Fig. 1C-D, Supplementary Fig. 2C-D) and caspse-3 activation (Supplementary Fig. 3). In order to rule out the possibility that apoptotic cell death was simply delayed in the absence of caspase-3, we further quantified the number of TUNEL^{+} cells in embryos collected 48 h following cisplatin treatment. While a small population of TUNEL^{+} cells were observed in *Casp3*$^{-/-}$ embryos at this time point, there remained a very significant (>90%) reduction in this population compared to that seen in both WT and *Casp3* heterozygous embryos (Fig. 2).

Given the proliferative nature of developing neuroepithelium during this period, we also examined the effect of cisplatin on cellular replication, quantifying Ki-67^{+} cell populations in treated embryos following cisplatin or vehicle treatment. No significant differences were observed in numbers of Ki-67^{+} cells in the developing brains of saline-treated WT, *Casp3*$^{+/-}$, and *Casp3*$^{-/-}$ embryos (Fig. 3, Supplementary Fig. 4). Similar to the results seen above, loss of caspase-3 prevented the substantial reduction in Ki-67^{+} populations seen in WT and *Casp3* heterozygous littermates following cisplatin treatment (Fig. 3). Thus, despite the cellular insults which may have been induced following cisplatin treatment, *Casp3*$^{-/-}$ neuroepithelia not only survived but were sufficiently intact to undergo cellular replication with no significant change in mitotic potential compared to vehicle-treated controls. Similarly, neuronal migration was not affected as no alteration in the pattern of cortical lamination was observed (Supplementary Fig. 5).

2.2. Loss of caspase-3 does not alter upstream DNA damage responses following cisplatin treatment

Since cell proliferation was not significantly affected by cisplatin treatment in *Casp3* null embryos, we next examined the nature of the DNA damage response initiated following cisplatin treatment in the absence of caspase-3. At 24 h following cisplatin treatment, we observed no differences in p53 levels between developing brains of *Casp3*$^{+/-}$ and *Casp3*$^{-/-}$ embryos (Fig. 4). Given that no detectable differences in p53 levels were observed at this time point between cisplatin and vehicle-treatment groups (Fig. 4A and B), we also examined induction of the cyclin-dependent kinase inhibitor p21 known to be transcriptionally activated *via* p53-dependent and independent mechanisms (Zamble et al., 1998). Notably, p21 was induced by cisplatin treatment and was observed to be unaffected by caspase-3 deletion (Fig. 4A and C); suggesting that it was activated independently of p53 in developing neuroepithelium. We further investigated the cisplatin-induced DNA damage response directly by examining induction of phospho-histone H2A.X (γ-H2A.X) (Mah et al., 2010). As shown in Fig. 5A and B, immunohistochemical analyses revealed a dramatic increase in histone H2A.X phosphorylation following cisplatin treatment in *Casp3* heterozygotes, with a reduced but similarly broad increase within the cortex of

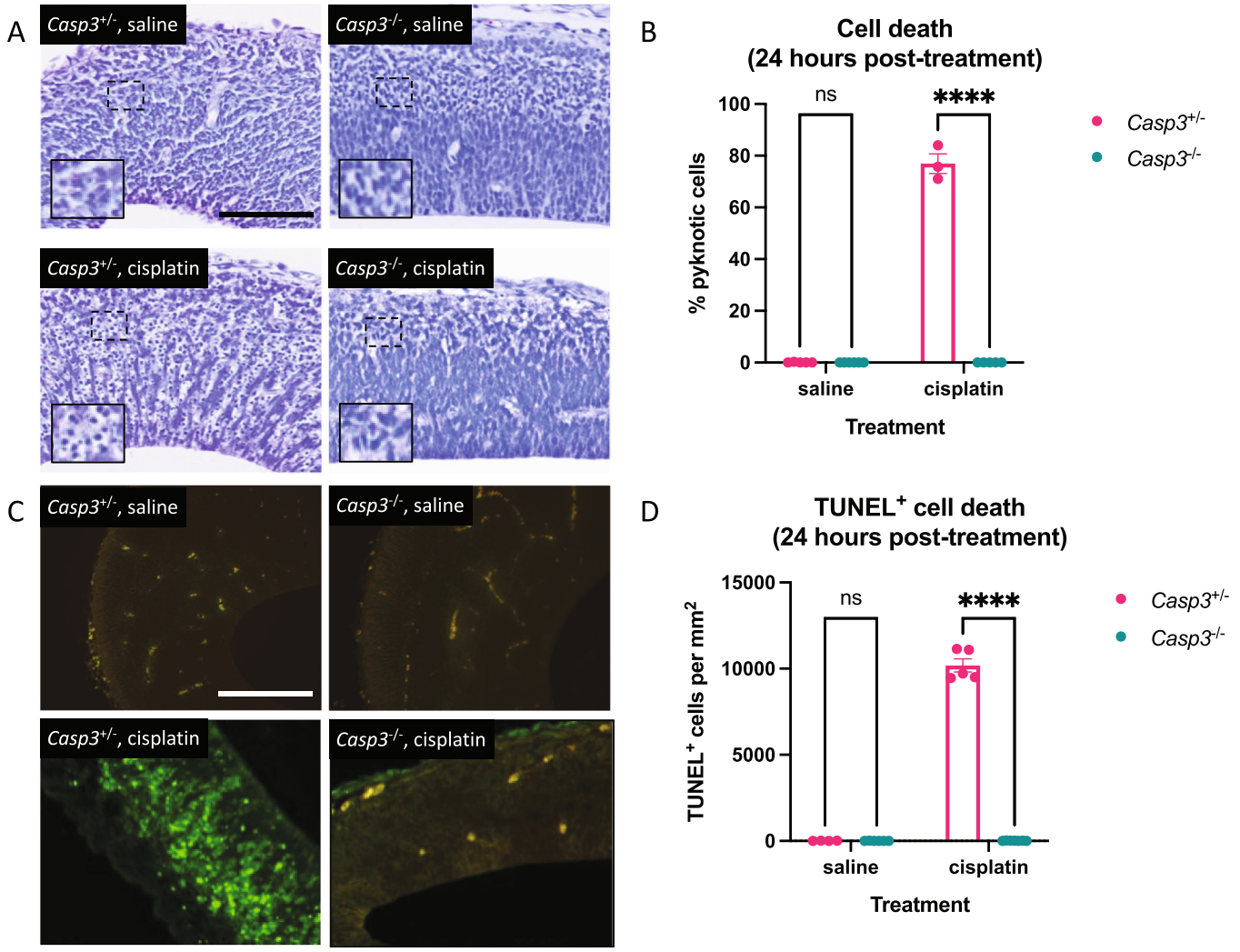

Fig. 1. *Casp3* deletion completely abolished cisplatin-induced cell death in the developing neuroepithelium.
A. Representative images of thionin-stained sections from the indicated treatment groups at 24 h following treatment. Insets: high magnification closeups of pyknotic cells with condensed nuclei observed in cisplatin-treated *Casp3*$^{+/-}$ animals whereas such cell populations are largely absent from other treatment groups.
B. Quantification of pyknotic cells in the germinal and early neuroepithelial layers of the developing neocortex at 24 h following the indicated treatment. $n = 5$ (*Casp3*$^{+/-}$, saline), $n = 6$ (*Casp3*$^{-/-}$, saline), $n = 3$ (*Casp3*$^{+/-}$, cisplatin), n = 5 (*Casp3*$^{-/-}$, cisplatin).
C. Representative images of fluorescent TUNEL staining from the indicated treatment groups at 24 h following treatment. Green channel represents TUNEL signal and red channel represents autofluorescence signal.
D. Quantification of TUNEL^{+} cells in the germinal and early neuroepithelial layers of the developing neocortex at 24 h following the indicated treatment. $n = 4$ (*Casp3*$^{+/-}$, saline), n = 6 (*Casp3*$^{-/-}$, saline), n = 5 (*Casp3*$^{+/-}$, cisplatin), $n = 7$ (*Casp3*$^{-/-}$, cisplatin).
**** $p < 0.0001$, ns indicates not statistically significant, two-way ANOVA with Bonferroni's multiple comparisons test.
Scale bars, 100 μm (A and C). (For interpretation of the references to colour in this figure legend, the reader is referred to the web version of this article.)

Casp3 null embryos (Fig. 5A). No significant differences in DNA damage response as measured by γ-H2A.X were observed between genotypes (Fig. 5B). The similar activities of p53 and p21 levels, and H2A.X phosphorylation suggest that the DNA damage response triggered by cisplatin treatment was largely unaffected by *Casp3* deletion, and as such the observed reduction in cisplatin-induced PCD was unlikely to be driven by differences in the initial responses of the developing neuroepithelia to cisplatin-induced DNA damage.

2.3. *Protection from cisplatin PCD following loss of caspase-3 is not the result of inhibited downstream apoptotic signalling*

As our results suggested that cisplatin-induced PCD in the absence of caspase-3 was not the result of a dampened DNA damage response, we next examined whether post-mitochondrial apoptotic signalling cascade was diminished in the absence of caspase-3. Previous *in cellulo* studies from our laboratory have demonstrated that caspase-3 is the predominant executioner caspase which can act to amplify caspase-7 signalling (Hui et al., 2011). Therefore, we examined caspase-7 levels and activation in WT, *Casp3*$^{+/-}$, and *Casp3*$^{-/-}$ embryos following cisplatin treatment. As shown in Fig. 6A and C, levels of procaspase-7 was largely unaffected by cisplatin treatment or the loss of caspase-3. Though cleavage of procaspase-7 to its active form was increased following cisplatin treatment, no significant differences were observed between the genotypes examined (Fig. 6A and D). To assess total executioner caspase activity, poly (ADP-ribose) polymerase (PARP) cleavage was quantified (Chaitanya et al., 2010; Hui et al., 2011). Consistent with the observations seen for caspase-7, PARP cleavage was induced by cisplatin treatment but similarly unaffected by the loss of caspase-3 (Fig. 6B and E, Supplementary Fig. 6). We further examined the extent of chromosomal DNA degradation to nucleosomal fragments as regulated by caspase-activated DNase (CAD). As shown in Fig. 6F, DNA laddering

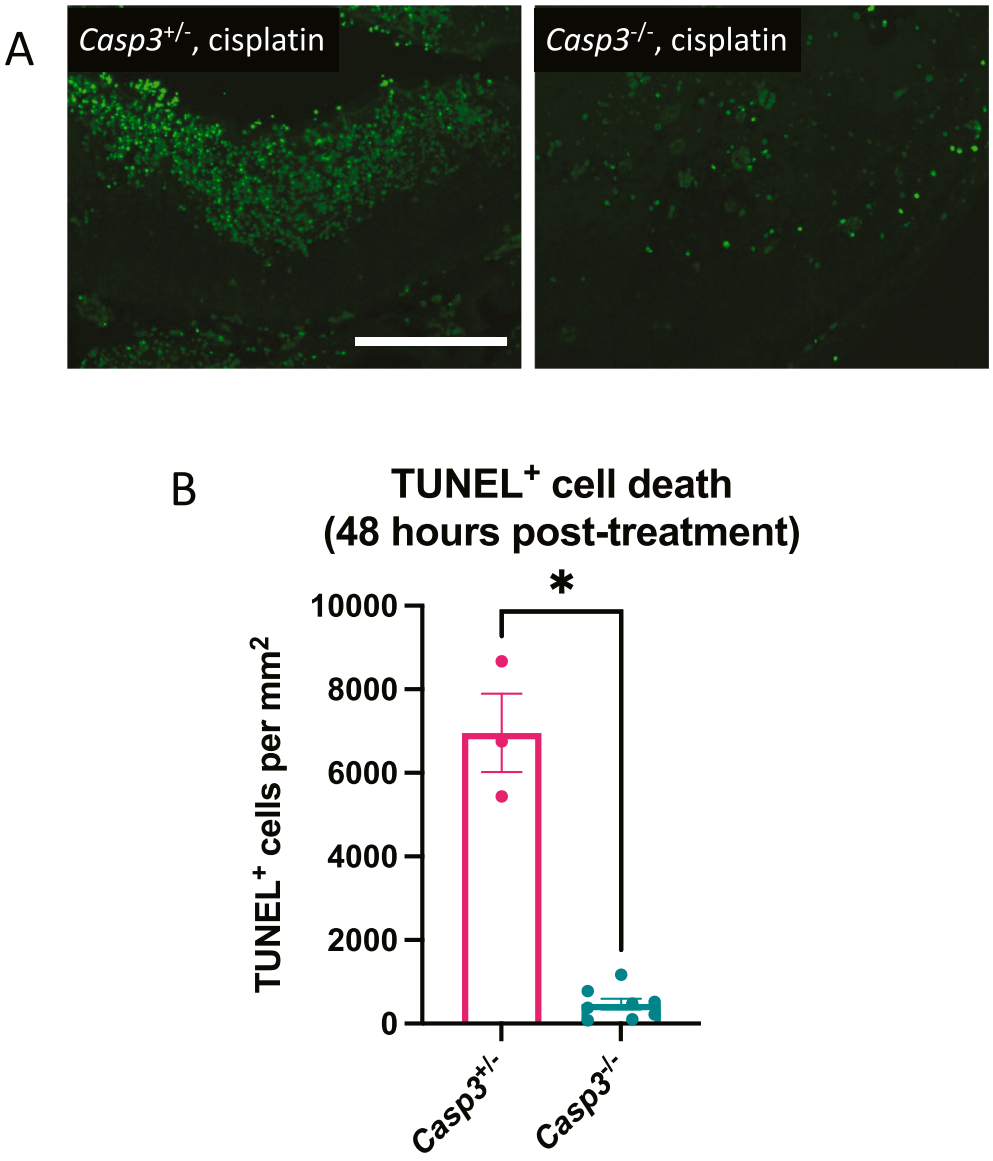

Fig. 2. Apoptotic cell death remained suppressed by *Casp3* deletion at 48 h post-cisplatin treatment.

A. Representative images of fluorescent TUNEL staining from the indicated treatment groups at 48 h following cisplatin treatment. Green channel represents TUNEL signal and red channel represents autofluorescence signal.

B. Quantification of TUNEL^{+} cells in the germinal and early neuroepithelial layers of the developing neocortex at 48 h following cisplatin treatment. n = 3 (*Casp3*$^{+/-}$, cisplatin), *n* = 8 (*Casp3*$^{-/-}$, cisplatin).

* $p < 0.05$, unpaired two-tailed Student's *t*-test with Welch's correction.

Scale bars, 100 μm (A). (For interpretation of the references to colour in this figure legend, the reader is referred to the web version of this article.)

indicative of chromosomal DNA degradation by CAD was observed in cisplatin-treated cortical samples obtained from *Casp3* WT or heterozygotes. Consistent with ICAD being a known caspase-3 specific substrate (Wolf et al., 1999), such nucleosomal DNA laddering was completely absent in cortical samples from cisplatin-treated *Casp3* null embryos. Together, these data suggest that the downstream apoptotic signalling cascade induced following cisplatin treatment *in vivo* was largely unaffected by the loss of caspase-3. However, despite the presence of caspase-7 activity and comparatively normal levels of executioner caspase activity (as determined by PARP cleavage), loss of caspase-3 resulted in a near complete abolition of programmed cell death within the developing neuroepithelium following cisplatin treatment at E12.5, highlighting the unique role of this caspase among executioner caspases in mitigating DNA damage-induced apoptosis *in vivo*.

2.4. Reduction of caspase-3 activity promotes an alternative form of PCD upon cisplatin treatment

Given the lack of changes in apoptotic signalling described above together with the suppression of cell death seen in *Casp3* null embryos in the presence of cisplatin, we attempted to understand the mechanism of cell death in developing cortical neuroepithelia through an examination of cell ultrastructure. As shown in Fig. 7A, no significant differences in cell ultrastructure was observed in vehicle-treated *Casp3*$^{+/+}$, *Casp3*$^{+/-}$, or *Casp3*$^{-/-}$ neuroepithelia. As expected, *Casp3* null embryos exhibited very low levels of cell death of any type either 24 or 48 h following cisplatin treatment (Fig. 7B and C). However, at 48 h post-treatment, small numbers of *Casp3* null cells (<2%) exhibit signs of structural necroptosis with cytoplasmic vacuolation and overt membrane degranulation (Fig. 7C right panel, green arrowheads) not seen in *Casp3*$^{+/+}$ neuroepithelia undergoing cell death (Fig. 7B left panel). Intriguingly, despite similar levels of overall cell death to that seen in *Casp3*$^{+/+}$ embryos, *Casp3*$^{+/-}$ neuroepithelial populations also exhibited some degree of this form of cell death at both 24 and 48 h post-treatment (Fig. 7B and C middle panels, respectively, green arrowheads). These findings suggests that the reduction in caspase-3 activity seen in *Casp3*$^{+/-}$ embryos is sufficient to promote either necroptosis or a hybrid form of necroptotic/apoptotic PCD in these tissues. That such programmed cell death is directly linked to caspase-3 activity is supported by the substantial reduction in both overall cell death and the necroptotic phenotype observed in *Casp3* null embryos.

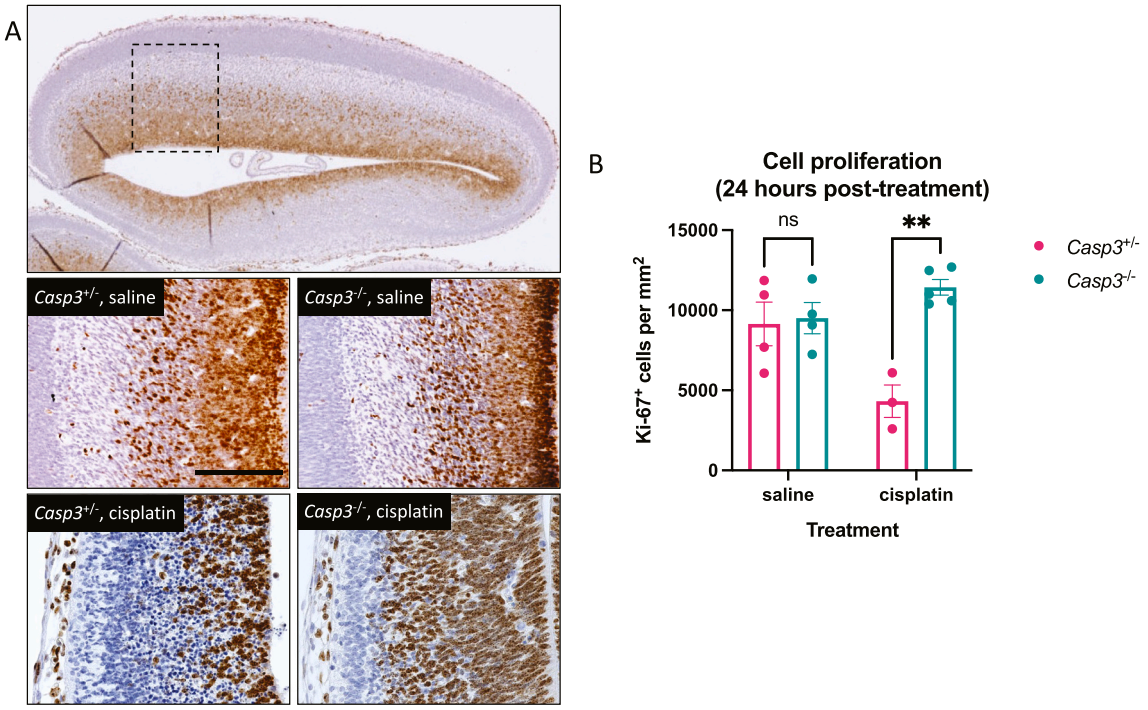

Fig. 3. Cisplatin treatment significantly diminished cell proliferation in the developing neuroepithelia of controls but was unaffected in *Casp3*$^{-/-}$ embryos.
A. Representative images of Ki-67 immunohistochemical staining from indicated treatment groups 24 h following treatment. Top: overview image to illustrate the region in which Ki-67^{+} cells were quantified.
B. Quantification of proliferating cells in the germinal and early neuroepithelial layers of the developing neocortex at 24 h following the indicated treatment. n = 4 (*Casp3*$^{+/-}$, saline), n = 4 (*Casp3*$^{-/-}$, saline), n = 3 (*Casp3*$^{+/-}$, cisplatin), n = 5 (*Casp3*$^{-/-}$, cisplatin).
** $p < 0.01$, ns indicates not statistically significant, two-way ANOVA with Bonferroni's multiple comparisons test.
Scale bars, 100 μm (A).

3. Discussion

In this study, we demonstrated that the *in vivo* toxicity of cisplatin on neural progenitor cells is completely dependent on caspase-3. During embryonic development, most regions of the brain are known to produce approximately twice the number of neurons than are ultimately incorporated into the network architecture. It was previously demonstrated that the selective removal of suboptimal targets and target-locus matching that helps to refine brain connectivity are largely mediated by apoptosis, but could be completed in the absence of caspase-3 due to compensation by the paralogue executioner caspase, caspase-7 (Houde et al., 2004; Woo et al., 1998). In contrast, our experiments have demonstrated cisplatin-induced cell death to be almost entirely abrogated by the deletion of *Casp3*. By examining cell death *via* quantifications of both pyknotic and TUNEL^{+} cells, we revealed that not only did the loss of caspase-3 result in a near-complete suppression of apoptosis, but cell death in general, as triggered by cisplatin-induced DNA damage. In fact, C*asp3*$^{-/-}$ animals were unexpectedly observed to survive to birth following *in utero* cisplatin treatment while control embryos could not be found during late embryonic development (E17.5) or postnatally (Supplementary Table 1). Furthermore, an in-depth analysis of WT embryos on either C57BL/6 J or CD-1 backgrounds collected at different time points similarly failed to identify any viable embryos beyond E16.5 (96 h post-cisplatin treatment) ($n = 7$ litters). Altogether, it would appear that not only does *Casp3* deletion provide protective effects at the cellular level against cisplatin toxicity but possibly at the organismal level as well. It will be of interest to determine whether such surviving pups could proceed properly with postnatal neurodevelopment and remain healthy into adulthood.

We further demonstrated that caspase-3 deficiency did not result in any significant changes to the cisplatin-induced DNA damage response or apoptotic signalling cascade by examining upstream pathways such as histone H2A.X phosphorylation, p53/p21 induction, caspase-7 levels/activation, and PARP cleavage. Surprisingly, cell proliferation, as measured by Ki-67-immunopositivity, was unaffected in the developing brains of *Casp3*$^{-/-}$ embryos despite substantial DNA damage experienced by the affected cells, indicated by histone H2A.X phosphorylation and p21 induction. The data thus suggest that the affected neural progenitor cells were able to enter mitosis in the absence of caspase-3. The observed live births of *Casp3*$^{-/-}$ pups following *in utero* cisplatin treatment consistently suggest perhaps that the affected cells are capable of performing DNA repair to be able to continue on with neurodevelopment once the apoptotic process was halted at the level of executioner caspase activation, commonly regarded as a "point of no return" for apoptotic cell death. It should be noted, however, that Ki-67 is expressed by all cells outside of G1 and G0 phases (Miller et al., 2018), therefore further experiments using phase-specific markers are necessary to determine whether the loss of caspase-3 indeed allowed the affected cells to proceed through cell cycle checkpoints without interruption despite having sustained significant DNA damage.

Interestingly, we were able to observe ultrastructural changes by electron microscopy to indicate that some affected cells in the developing neuroepithelium were exhibiting signs of necroptosis. Consistent with such observations, genetic and chemical means of necroptosis inhibition have been shown previously to diminish cisplatin-induced toxicity (Jing et al., 2018; Sun et al., 2018; Wang et al., 2019; Xu et al., 2017; Zheng et al., 2020). However, it seems likely that necroptotic signalling was initiated in a stochastic manner when apoptotic cell death was blocked, given that not all affected cells displayed signs of necroptosis when caspase-3 was absent and that most cells continued to live and proliferate. It will therefore be of interest to determine whether cisplatin-mediated cell killing predominantly triggers apoptosis in most cells but also simultaneously initiate necroptosis in others, albeit to a lesser extent, or that a subpopulation of cells triggers necroptosis

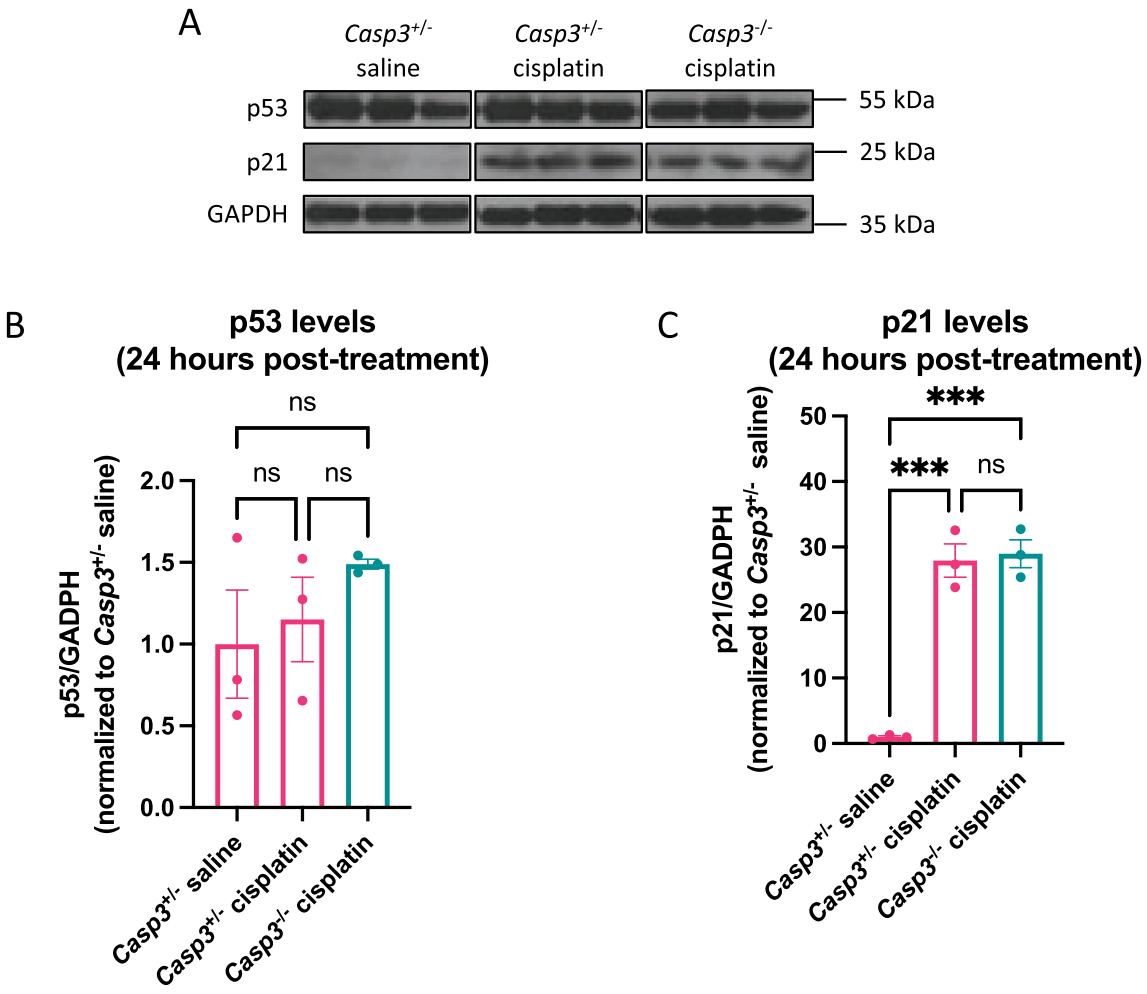

Fig. 4. Induction of DNA damage response was unaffected by *Casp3* deletion.
A. Representative blot images of p53 and p21 from the indicated treatment groups at 24 h following treatment.
B. Quantification of normalized p53 levels from the indicated treatment groups at 24 h following treatment. n = 3 (*Casp3*$^{+/-}$, saline), n = 3 (*Casp3*$^{+/-}$, cisplatin), n = 3 (*Casp3*$^{-/-}$, cisplatin).
C. Quantification of normalized p21 levels from the indicated treatment groups at 24 h following treatment. n = 3 (*Casp3*$^{+/-}$, saline), n = 3 (*Casp3*$^{+/-}$, cisplatin), n = 3 (*Casp3*$^{-/-}$, cisplatin).
*** $p < 0.001$, ns indicates not statistically significant, one-way ANOVA with Bonferroni's multiple comparisons test.

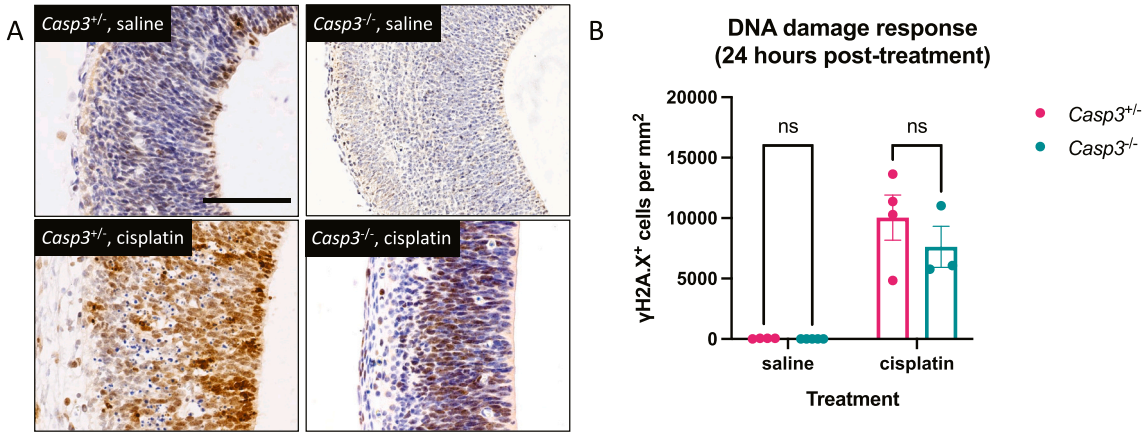

Fig. 5. Recognition of DNA damage was unaffected by *Casp3* deletion.
A. Representative images of phosphorylated histone H2A.X immunohistochemical staining from the indicated treatment groups at 24 h following treatment.
B. Quantification of γ-H2A.X^{+} cells in the germinal and early neuroepithelial layers of the developing neocortex at 24 h following the indicated treatment. n = 4 (*Casp3*$^{+/-}$, saline), n = 5 (*Casp3*$^{-/-}$, saline), n = 4 (*Casp3*$^{+/-}$, cisplatin), n = 3 (*Casp3*$^{-/-}$, cisplatin).
ns indicates not statistically significant, two-way ANOVA with Bonferroni's multiple comparisons test.
Scale bars, 100 μm (A).

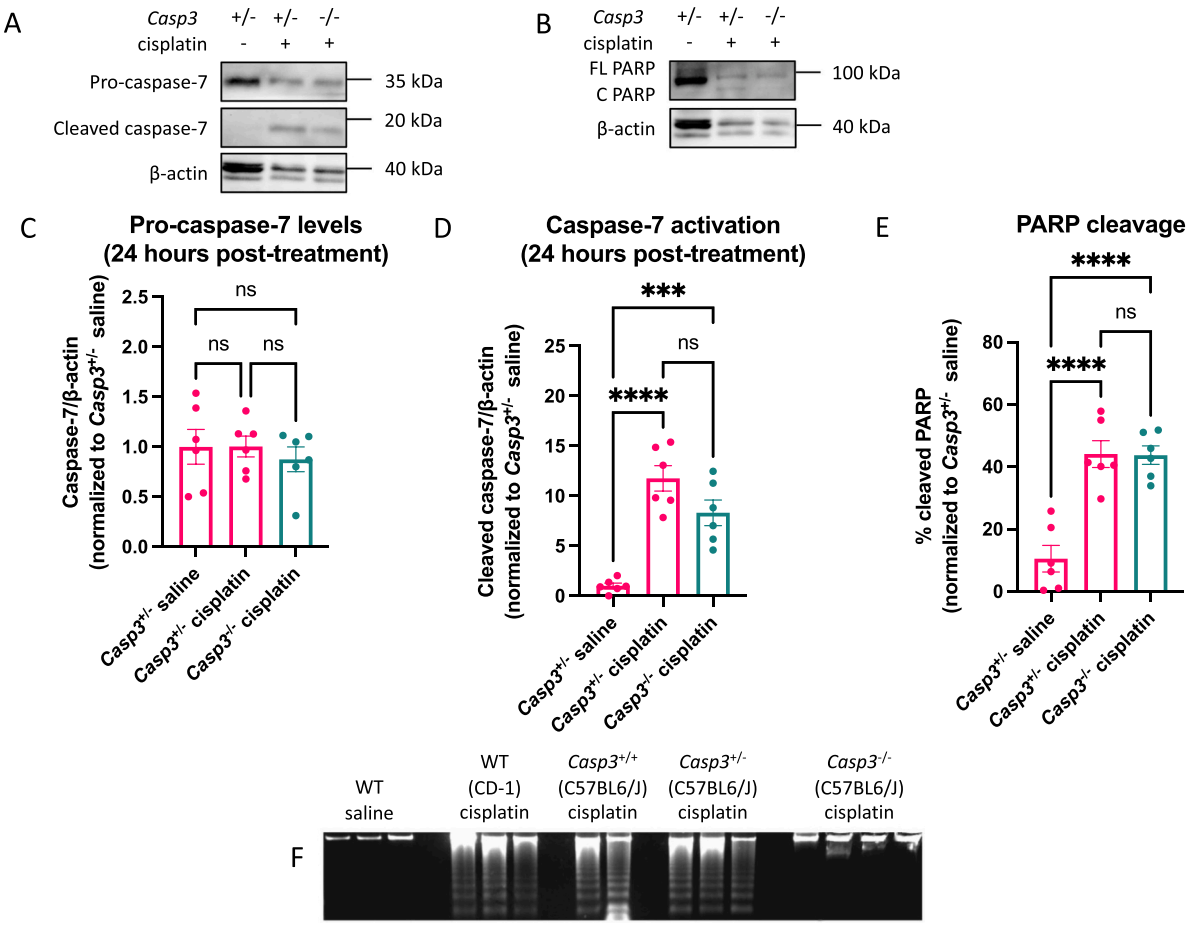

Fig. 6. *Casp3* deletion did not affect apoptotic signalling cascade in the developing neuroepithelium.
A. Representative blot images of full-length and cleaved caspase-7 from the indicated treatment groups at 24 h following treatment.
B. Representative blot images of full-length and cleavage PARP from the indicated treatment groups at 24 h following treatment.
C. Quantification of normalized caspase-7 levels from the indicated treatment groups at 24 h following treatment. n = 6 ($Casp3^{+/-}$, saline), n = 6 ($Casp3^{+/-}$, cisplatin), n = 6 ($Casp3^{-/-}$, cisplatin).
D. Quantification of normalized caspase-7 activation from the indicated treatment groups at 24 h following treatment. n = 6 ($Casp3^{+/-}$, saline), n = 6 ($Casp3^{+/-}$, cisplatin), n = 6 ($Casp3^{-/-}$, cisplatin).
E. Quantification of normalized PARP cleavage (cleaved PARP as a percentage of the sum of full-length and cleaved PARP) from the indicated treatment groups at 24 h following treatment. n = 6 ($Casp3^{+/-}$, saline), n = 6 ($Casp3^{+/-}$, cisplatin), n = 6 ($Casp3^{-/-}$, cisplatin).
F. Representative gel images of DNA laddering from the indicated treatment groups at 24 h following treatment.
*** $p < 0.001$, **** $p < 0.0001$, ns indicates not statistically significant, one-way ANOVA (C and E) or Brown-Forsythe one-way ANOVA (D) with Bonferroni's multiple comparisons test. (For interpretation of the references to colour in this figure legend, the reader is referred to the web version of this article.)

secondarily to failed apoptosis as they have sustained irreparable cellular damage. Although we did not quantitatively examine ultrastructural changes associated with necroptotic cell death across the entire developing neuroepithelium in this study, our observations suggest that the latter is more likely as necroptotic cells were observed only when the gene dosage of *Casp3* was reduced and not readily identified in WT embryos. Furthermore, we were unable to observe any significant changes in necroptotic signalling even in $Casp3^{-/-}$ embryos (data not shown), further highlighting that it was unlikely to have been activated only to be masked by the massive activation of apoptosis caused by cisplatin treatment.

Our findings from this study indicate that caspase-3-mediated apoptotic cell death is uniquely required for cisplatin-mediated cytotoxicity. This is in contrast to a variety of reports which have inferred to an overlapping role for caspase-3 and -7 (Hui et al., 2011; Lakhani et al., 2006), and consistent with studies which suggest the two to possess distinct functions (Walsh et al., 2008). Notably, we observed PARP cleavage to occur in response to cisplatin treatment despite the absence of caspase-3, thus indicating an adequate amount of "common" executioner caspase activity. Conversely, DNA laddering was not observed in $Casp3^{-/-}$ embryos, thus indicating that ICAD likely had remained intact and functional to prevent nucleosomal degradation by CAD. Therefore, the differential requirement for caspase-3 in cisplatin-induced and naturally occurring apoptotic cell death likely rests upon the distinct list of substrates and downstream processes altered only by caspase-3 activity and thus are necessary for cisplatin-mediated cytotoxicity but dispensable for apoptotic cell death designed to trim and shape the developing brain. Furthermore, it will be of interest to determine the extent with which *Casp3* deletion protects other cell/tissue types against DNA damage-induced toxicity by cisplatin and related cytotoxic drugs as it will provide new mechanistic insights into why certain tissues exhibit enhanced sensitivity to cisplatin treatment and limit its clinical applications.

4. Materials and methods

4.1. Animals and treatment

Casp3 mutant animals were backcrossed >7 generations and maintained on a C57BL/6 J background. Genotyping of parental crosses was

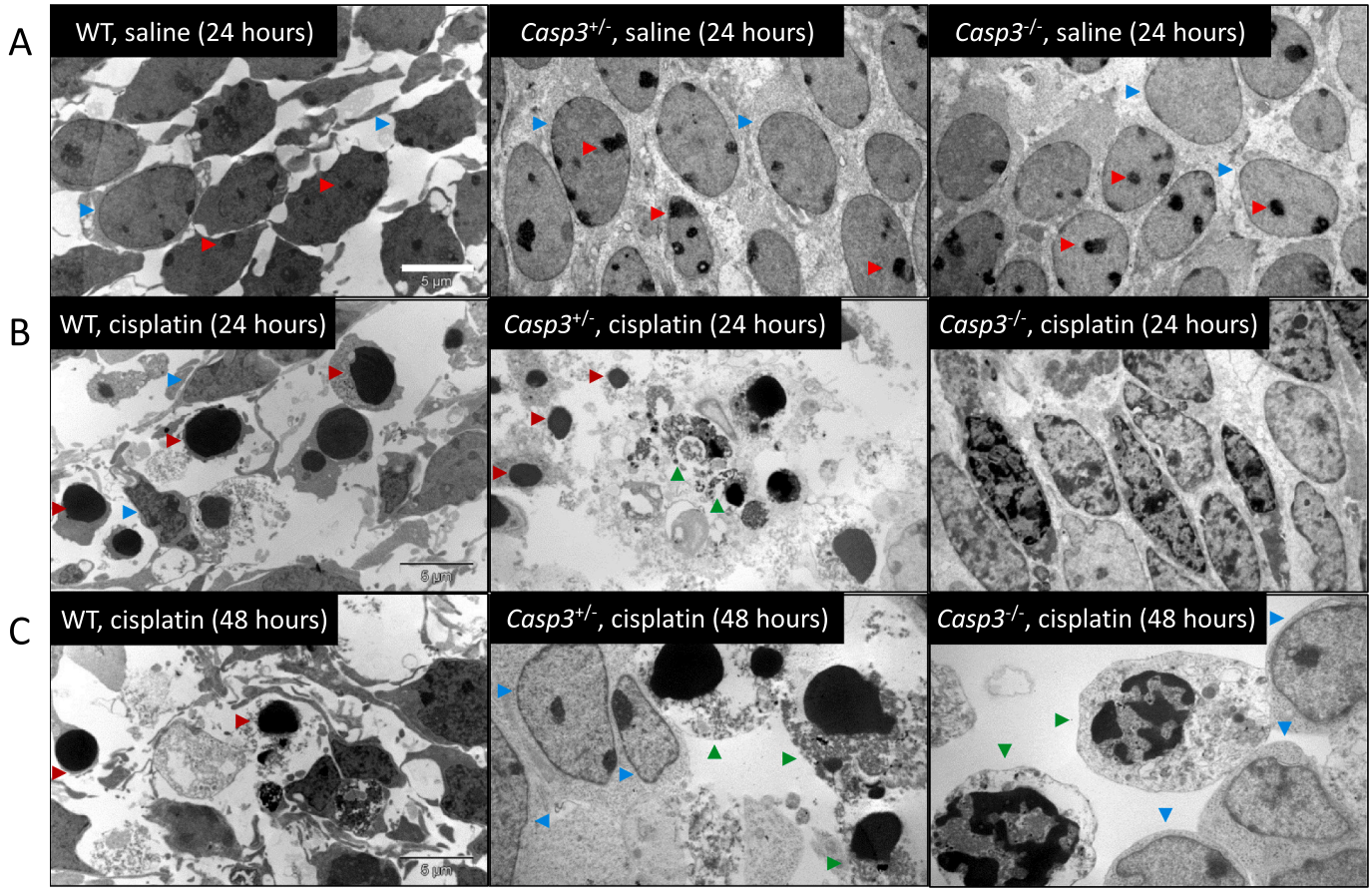

Fig. 7. Some cells in the developing neuroepithelia of *Casp3*$^{-/-}$ embryos exhibited signs of necroptotic cell death.
A. Representative electron micrographs within the dense zone of developing neuroepithelium in saline control group of each genotype. Examples of relative position of the nuclear envelope (blue arrowhead) are shown, together with regions of dense chromatin staining (red arrowhead) surrounded by light (eu-) chromatin regions.
B. Cellular appearance of neuroepithelia at 24 h following cisplatin treatment for each of the identified genotypes. Nuclei of wild-type embryos demonstrate classic apoptotic features (amber arrowheads) which have begun to collapse into apoptotic bodies. Nuclei of several surviving neuroepithelia are also indicated (blue arrowheads). *Casp3*$^{+/-}$ embryos also exhibit apoptotic nuclear features (amber arrowheads) and cells exhibiting necrotic features (green arrowheads). By contrast, *Casp3*$^{-/-}$ embryos exhibit large number of cells with intact nuclear profiles.
C. Representative electron photomicrographs of the developing neuroepithelium at 48 h following cisplatin treatment. Wild-type neuroepithelia exhibit apoptosis (amber arrowheads) with late-stage degeneration. *Casp3*$^{+/-}$ embryos exhibit apoptotic bodies with necrotic features (green arrowheads) together with intact nuclear profiles (blue arrowheads). *Casp3*$^{-/-}$ embryos exhibit intact nuclear profiles (blue arrowheads), together with cells exhibiting intact cellular membranes but condensed chromatin with some necrotic features.
Scale bars, 5 µm (A to C). (For interpretation of the references to colour in this figure legend, the reader is referred to the web version of this article.)

performed by PCR on genomic DNA isolated from tail clippings. Breeding pairs were typically arranged such that male mice heterozygous or homozygous null for *Casp3* were interbred with heterozygous females. To assess the potential effects of genetic background, embryos on both the outbred CD-1 and the inbred C57BL/6 J strain were utilized. Timed matings were performed by housing male mice overnight with between one and three females with plugs checked the next morning designated as embryonic day 0.5 (E0.5). Pregnancy was further monitored by relative weight gain of females and pregnant dams were treated randomly with either vehicle (saline) or cisplatin. Cisplatin was freshly dissolved in 0.9% normal saline and administered intraperitoneally at a dose of 20 mg/kg in a total volume of 300–500 µL on E12.5. Based upon FDA accepted bio-comparisons, this dosage corresponds to a human equivalent dose of approximately 60 mg/m^2, slightly below typical clinical dosages used in humans (80–120 mg/m^2). Upon sacrifice, animals were anesthetized using isofluorane and killed by cervical dislocation at the indicated time points. Embryos were excised and relevant tissues initially dissected in phosphate-buffered saline (PBS). Embryos were individually genotyped by PCR where necessary. Experimenters for subsequent analyses were not blinded to the genotype information of the samples following genotyping. Animals were provided rodent chow and tap water *ad libitum*. All work was performed in accordance with Canadian Council of Animal Care and University of Toronto guidelines.

4.2. Tissue processing and immunohistochemistry

Following dissection and harvesting of the relevant tissues, samples were frozen or immediately placed in 4% paraformaldehyde in PBS and fixed with gentle agitation at 4 °C. Tissues were then processed through a series of ethanol, xylene, and paraffin baths and embedded in paraffin wax. Blocks were cut in horizontal, coronal, or sagittal planes on a Leica microtome at a thickness of 7 µm. Sections were mounted onto poly-L-lysine coated slides and melted overnight at 65 °C. Paraffin sections were subsequently de-waxed and rehydrated in a series of xylene, ethanol, and water baths. Thionin-stained sections were used for assessment of general histology. For immunohistochemical studies, sections were washed in PBS and exposed to 0.3% hydrogen peroxide in PBS for 30 min to destroy endogenous peroxidase activity (Hui et al., 2010). Sections were washed thrice with PBS and antigen retrieval performed as needed, consisting of immersion of slides into 10 mM sodium citrate, pH 6, and microwaved for 10–15 min in a pre-warmed water-filled pressure cooker until pressure was attained. Power was

then decreased by 50% and the vessel heated for an additional 5 min. Following incubation in a cold water bath to reduce the pressure, the chamber was opened and slides were allowed to cool completely and washed with PBS before primary antisera were applied. Antisera were diluted in PBS (Supplementary Table 2) containing 3% bovine serum albumin (BSA), 20 mM $MgCl_2$, 0.3% Tween-20, 0.2% Triton X-100, and 5% appropriate serum and applied to the slides. Slides were incubated overnight at 4 °C in a humidity chamber. The slides were brought to room temperature the following day and washed once with PBS containing 0.3% Triton X-100 (TBS-T) and thrice with PBS. Secondary antisera were diluted in PBS containing 0.2% Triton X-100 and applied to sections for 1–2 h at room temperature with gentle agitation. Following a wash in PBS-T and three washes in PBS, avidin-biotin horseradish peroxidase complex was applied for 1 h at room temperature in accordance with the manufacturer's instructions (ABC Vectastain Elite Kit, Vector Labs). Sections were washed once in PBS-T, thrice in PBS, and once in 100 mM Tris-Cl, pH 7.5 before being developed in diaminobenzidine (DAB) for 4–5 min to visualize peroxidase activity. Where necessary, hematoxylin was used as a counterstain. Sections were dehydrated back in xylene and cover slipped using xylene-based mounting media (Permount, Sigma-Aldrich).

4.3. TUNEL assay

Terminal deoxynucleotidyl transferase-mediated nick end labeling (TUNEL) targets 3'-OH overhangs characteristic of DNA strand breaks produced during apoptosis and so was used to identify apoptotic cells together with electron microscopy. Paraffin sections were de-waxed and rehydrated as indicated above and washed once in PBS, followed by an incubation in pre-warmed 10 mM Tris (pH 7.5) containing 20 μg/mL proteinase K, at 37 °C for 20 min. Following three washes with PBS, the sections were incubated with FITC-labelling constituents in the presence of terminal deoxynucleotidyl transferase (TdT) according to the manufacturer's instructions (Roche Diagnostics). Sections were mounted with Vectashield (Vector Labs) for examination *via* epifluorescence.

4.4. Western blotting

Embryonic brains were dissected in PBS, flash frozen in liquid nitrogen, and stored at −80 °C until homogenized. Tissues were homogenized by pipette in 200–300 μL of ice-cold radioimmunoprecipitation assay (RIPA) lysis buffer supplemented with protease inhibitors (20 mM Tris-HCl, pH 7.5, 150 mM NaCl, 1 mM Na_2EDTA, 1 mM EGTA, 1% NP-40, 1% sodium deoxycholate, 2.5 mM sodium pyrophosphate, 1 mM β-glycerophosphate, 1 mM Na_3VO_4, 1 μg/mL leupeptin; Cell Signaling Technology). Following centrifugation, protein concentration was determined by bicinchoninic acid (BCA) assay against a bovine serum albumin (BSA) standard of known concentrations. Depending upon the experiment, 40–60 μg of total protein for each sample was separated on 10% or 12% SDS-PAGE gels and transferred onto nitrocellulose membranes using a wet transfer apparatus. Membranes were blocked with 5% powdered skim milk in TBS-T for 1 h and incubated in primary antisera overnight at 4 °C with gentle agitation. Following three washes in TBS-T, membranes were incubated for 1–2 h with the appropriate horseradish peroxidase-conjugated secondary antibodies at 4 °C. Membranes were washed thrice in TBS-T and peroxidase activity was determined using standard ECL procedures (SuperSignal West Pico, Thermo Fisher Scientific). Blots were developed on film and protein levels were quantified based on densitometry normalized to β-actin or GAPDH loading controls using ImageJ software.

4.5. DNA fragmentation assay

Individual embryonic brains were dissected in PBS and DNA isolated by overnight incubation in 0.5 mL lysis buffer (50 mM Tris-HCl, pH 8, 100 mM EDTA, 100 mM NaCl, 1% SDS, containing 1 mg/mL freshly added proteinase K) overnight at 65 °C. Twenty microliters of 10 mg/mL RNAse was added to lysates the following day and incubated for 1–2 h at 37 °C. Two hundred microliters of 5 M NaCl and 700 μL of chloroform were sequentially added to the lysates and were centrifuged at 10,000 $\times g$ for 10 min at 4 °C. The aqueous phase was transferred to a new tube and topped up with ice cold 100% ethanol to precipitate genomic DNA, followed by centrifugation at 10,000 $\times g$ for 10 min at 4 °C. Pellets were washed with ice-cold 70% ethanol, allowed to air dry, and dissolved in 30–50 μL Tris-EDTA. DNA concentration was measured by Nanodrop and 3 μg was loaded onto a 1.5% agarose gel and visualized by ethidium bromide.

4.6. Electron microscopy

For electron microscopy embryonic brains were removed and the neocortex was dissected into 4% paraformaldehyde followed by fixing in glutaraldehyde at 4 °C overnight with gentle agitation. Tissues then underwent processing where they were post-fixed in 1% osmium tetroxide for 2 h and processed into Spurr resin. One micron thick sections were stained with toluidine blue and examined for Regions of Interest (ROI). Resin-embedded 70-nm sections were mounted on 200 mesh copper grids and stained with 2% uranyl acetate and 0.1% lead citrate. Electron microscopy was performed using a Philips CM 100 TEM fitted with a Kodak 1.4 megapixel digital camera.

4.7. Statistical analysis

No data were excluded from experimental and statistical analyses and as such no exclusion criteria were applied in this study. Statistical analyses were performed using GraphPad Prism 9.2.0. Results were presented as mean ± SEM. Statistics tests performed to test differences between means were described in the respective figure legends. Results were considered significant if $p < 0.05$.

4.8. Image acquisition

Brightfield images were obtained using a NanoZoomer 2.0 HT scanner software at 20× magnification. Fluorescent images were acquired using a Nikon Eclipse E-1000 microscope equipped with DAPI, FITC, GFP, TRITC, and CY5 epifluorescence excitation/emission filter sets using a Hamamatsu ORCA-285 camera. Where performed, images were only adjusted for brightness and contrast using Adobe Photoshop 7.0 and applied across the entire image frame.

Author contributions

Conceptualization: K.K.H., M.L., and J.T.H. Investigation and Validation: M.L., K.K.H., C.D.S., S.H., and C.E.R.Formal analysis: M.L. and K. K.H.Methodology and Resources: A.J.E. Visualization and Writing - original draft: K.K.H., M.L., J.T.H. Writing - review: K.K.H. and J.T.H.

Funding

This study was supported by grants awarded to J.T.H. from Natural Sciences and Engineering Research Council of Canada (NSERC) (RGPIN 298553-12). K.K.H. was supported by Canadian Institute of Health Research (CIHR)/Health Research Foundation (HRF) Graduate Scholarship in Pharmacy. C.D.S. was funded by Natural Sciences and Engineering Research Council of Canada (NSERC) and Queen Elizabeth II Graduate Scholarships in Science & Technology.

Data availability

All data generated or analyzed during this study are included in this published article [and its supplementary information files].

Declaration of Competing Interest

The authors declare no competing financial interests in relation to the work described.

Acknowledgements

We would like to thank Ali Darbandi and Doug Holmyard for assistance with electron microscopy.

Appendix A. Supplementary data

Supplementary data to this article can be found online at https://doi.org/10.1016/j.expneurol.2022.114010.

References

Awasthi, P., Foiani, M., Kumar, A., 2015. ATM and ATR signaling at a glance. J. Cell Sci. 128, 4255–4262. https://doi.org/10.1242/jcs.169730.

Blanc, C., Deveraux, Q.L., Krajewski, S., Jänicke, R.U., Porter, A.G., Reed, J.C., Jaggi, R., Marti, A., 2000. Caspase-3 is essential for procaspase-9 processing and cisplatin-induced apoptosis of MCF-7 breast cancer cells. Cancer Res. 60, 4386–4390.

Cecconi, F., Alvarez-Bolado, G., Meyer, B.I., Roth, K.A., Gruss, P., 1998. Apaf1 (CED-4 homolog) regulates programmed cell death in mammalian development. Cell 94, 727–737. https://doi.org/10.1016/s0092-8674(00)81732-8.

Chaitanya, G.V., Alexander, J.S., Babu, P.P., 2010. PARP-1 cleavage fragments: signatures of cell-death proteases in neurodegeneration. Cell Commun. Signal 8, 31. https://doi.org/10.1186/1478-811x-8-31.

Cummings, B.S., Schnellmann, R.G., 2002. Cisplatin-induced renal cell apoptosis: caspase 3-dependent and -independent pathways. J. Pharmacol. Exp. Ther. 302, 8–17. https://doi.org/10.1124/jpet.302.1.8.

Dasari, S., Tchounwou, P.B., 2014. Cisplatin in cancer therapy: molecular mechanisms of action. Eur. J. Pharmacol. 740, 364–378. https://doi.org/10.1016/j.ejphar.2014.07.025.

Dietrich, J., Han, R., Yang, Y., Mayer-Pröschel, M., Noble, M., 2006. CNS progenitor cells and oligodendrocytes are targets of chemotherapeutic agents in vitro and in vivo. J. Biol. 5, 22. https://doi.org/10.1186/jbiol50.

Hakem, R., Hakem, A., Duncan, G.S., Henderson, J.T., Woo, M., Soengas, M.S., Elia, A., de la Pompa, J.L., Kagi, D., Khoo, W., Potter, J., Yoshida, R., Kaufman, S.A., Lowe, S. W., Penninger, J.M., Mak, T.W., 1998. Differential requirement for caspase 9 in apoptotic pathways in vivo. Cell 94, 339–352. https://doi.org/10.1016/s0092-8674(00)81477-4.

Henkels, K.M., Turchi, J.J., 1999. Cisplatin-induced apoptosis proceeds by caspase-3-dependent and -independent pathways in cisplatin-resistant and -sensitive human ovarian cancer cell lines. Cancer Res. 59, 3077–3083.

Houde, C., Banks, K.G., Coulombe, N., Rasper, D., Grimm, E., Roy, S., Simpson, E.M., Nicholson, D.W., 2004. Caspase-7 expanded function and intrinsic expression level underlies strain-specific brain phenotype of Caspase-3-null mice. J. Neurosci. 24, 9977–9984. https://doi.org/10.1523/jneurosci.3356-04.2004.

Hui, K.K.W., Liadis, N., Robertson, J., Kanungo, A., Henderson, J.T., 2010. Calcineurin inhibition enhances motor neuron survival following injury. J. Cell. Mol. Med. 14, 671–686. https://doi.org/10.1111/j.1582-4934.2009.00715.x.

Hui, K.K.W., Kanungo, A.K., Elia, A.J., Henderson, J.T., 2011. Caspase-3 deficiency reveals a physiologic role for Smac/DIABLO in regulating programmed cell death. Cell Death Differ. 18, 1780–1790. https://doi.org/10.1038/cdd.2011.50.

Jing, L., Song, F., Liu, Z., Li, J., Wu, B., Fu, Z., Jiang, J., Chen, Z., 2018. MLKL-PITPα signaling-mediated necroptosis contributes to cisplatin-triggered cell death in lung cancer A549 cells. Cancer Lett. 414, 136–146. https://doi.org/10.1016/j.canlet.2017.10.047.

Kamarajan, P., Sun, N.-K., Sun, C.-L., Chao, C.C.-K., 2001. Apaf-1 overexpression partially overcomes apoptotic resistance in a cisplatin-selected HeLa cell line. FEBS Lett. 505, 206–212. https://doi.org/10.1016/s0014-5793(01)02817-4.

Kanungo, A.K., Liadis, N., Robertson, J., Woo, M., Henderson, J.T., 2009. Excitatory tonus is required for the survival of granule cell precursors during postnatal development within the cerebellum. Neuroscience 158, 1364–1377. https://doi.org/10.1016/j.neuroscience.2008.10.062.

Köpf-Maier, P., Merker, H., 1983. Effects of the cytostatic drug cis-platinum on the developing neocortex of the mouse. Teratology 28, 189–199. https://doi.org/10.1002/tera.1420280207.

Kuida, K., Zheng, T.S., Na, S., Kuan, C.-Y., Yang, D., Karasuyama, H., Rakic, P., Flavell, R. A., 1996. Decreased apoptosis in the brain and premature lethality in CPP32-deficient mice. Nature 384, 368–372. https://doi.org/10.1038/384368a0.

Kuida, K., Haydar, T.F., Kuan, C.-Y., Gu, Y., Taya, C., Karasuyama, H., Su, M.S.-S., Rakic, P., Flavell, R.A., 1998. Reduced apoptosis and cytochrome c–mediated caspase activation in mice lacking caspase 9. Cell 94, 325–337. https://doi.org/10.1016/s0092-8674(00)81476-2.

Lakhani, S.A., Masud, A., Kuida, K., Porter, G.A., Booth, C.J., Mehal, W.Z., Inayat, I., Flavell, R.A., 2006. Caspases 3 and 7: key mediators of mitochondrial events of apoptosis. Science 311, 847–851. https://doi.org/10.1126/science.1115035.

Mah, L.-J., El-Osta, A., Karagiannis, T.C., 2010. γH2AX: a sensitive molecular marker of DNA damage and repair. Leukemia 24, 679–686. https://doi.org/10.1038/leu.2010.6.

Miller, I., Min, M., Yang, C., Tian, C., Gookin, S., Carter, D., Spencer, S.L., 2018. Ki67 is a graded rather than a binary marker of proliferation versus quiescence. Cell Rep. 24, 1105–1112.e5. https://doi.org/10.1016/j.celrep.2018.06.110.

Minisini, A., Atalay, G., Bottomley, A., Puglisi, F., Piccart, M., Biganzoli, L., 2004. What is the effect of systemic anticancer treatment on cognitive function? Lancet Oncol. 5, 273–282. https://doi.org/10.1016/s1470-2045(04)01465-2.

Nakano, K., Vousden, K.H., 2001. PUMA, a novel proapoptotic gene, is induced by p53. Mol. Cell 7, 683–694. https://doi.org/10.1016/s1097-2765(01)00214-3.

Singh, R., Letai, A., Sarosiek, K., 2019. Regulation of apoptosis in health and disease: the balancing act of BCL-2 family proteins. Nat. Rev. Mol. Cell Biol. 20, 175–193. https://doi.org/10.1038/s41580-018-0089-8.

Sun, Y., Zhai, L., Ma, S., Zhang, C., Zhao, L., Li, N., Xu, Y., Zhang, T., Guo, Z., Zhang, H., Xu, P., Zhao, X., 2018. Down-regulation of RIP3 potentiates cisplatin chemoresistance by triggering HSP90-ERK pathway mediated DNA repair in esophageal squamous cell carcinoma. Cancer Lett. 418, 97–108. https://doi.org/10.1016/j.canlet.2018.01.022.

Toshiyuki, M., Reed, J.C., 1995. Tumor suppressor p53 is a direct transcriptional activator of the human bax gene. Cell 80, 293–299. https://doi.org/10.1016/0092-8674(95)90412-3.

Walsh, J.G., Cullen, S.P., Sheridan, C., Lüthi, A.U., Gerner, C., Martin, S.J., 2008. Executioner caspase-3 and caspase-7 are functionally distinct proteases. Proc. Natl. Acad. Sci. U. S. A. 105, 12815–12819. https://doi.org/10.1073/pnas.0707715105.

Wang, J., Liu, M., Wang, F., Wei, B., Yang, Q., Cai, Y., Chen, X., Liu, X., Jiang, L., Li, C., Hu, X., Yu, J., Ma, T., Jin, J., Wu, Y., Li, J., Meng, X., 2019. RIPK1 inhibitor Cpd-71 attenuates renal dysfunction in cisplatin-treated mice via attenuating necroptosis, inflammation and oxidative stress. Clin. Sci. 133, 1609–1627. https://doi.org/10.1042/cs20190599.

Wolf, B.B., Schuler, M., Echeverri, F., Green, D.R., 1999. Caspase-3 is the primary activator of apoptotic DNA fragmentation via DNA fragmentation Factor-45/inhibitor of caspase-activated DNase inactivation. J. Biol. Chem. 274, 30651–30656. https://doi.org/10.1074/jbc.274.43.30651.

Woo, M., Hakem, R., Soengas, M.S., Duncan, G.S., Shahinian, A., Kagi, D., Hakem, A., McCurrach, M., Khoo, W., Kaufman, S.A., Senaldi, G., Howard, T., Lowe, S.W., Mak, T.W., 1998. Essential contribution of caspase 3/CPP32 to apoptosis and its associated nuclear changes. Genes Dev. 12, 806–819. https://doi.org/10.1101/gad.12.6.806.

Xu, Y., Ma, H.-B., Fang, Y.-L., Zhang, Z.-R., Shao, J., Hong, M., Huang, C.-J., Liu, J., Chen, R.-Q., 2017. Cisplatin-induced necroptosis in TNFα dependent and independent pathways. Cell. Signal. 31, 112–123. https://doi.org/10.1016/j.cellsig.2017.01.004.

Yang, X., Zheng, F., Xing, H., Gao, Q., Wei, W., Lu, Y., Wang, S., Zhou, J., Hu, W., Ma, D., 2004. Resistance to chemotherapy-induced apoptosis via decreased caspase-3 activity and overexpression of antiapoptotic proteins in ovarian cancer. J. Cancer Res. Clin. 130, 423–428. https://doi.org/10.1007/s00432-004-0556-9.

Yoshida, H., Kong, Y.-Y., Yoshida, R., Elia, A.J., Hakem, A., Hakem, R., Penninger, J.M., Mak, T.W., 1998. Apaf1 is required for mitochondrial pathways of apoptosis and brain development. Cell 94, 739–750. https://doi.org/10.1016/s0092-8674(00)81733-x.

Zamble, D.B., Jacks, T., Lippard, S.J., 1998. p53-dependent and -independent responses to cisplatin in mouse testicular teratocarcinoma cells. Proc. Natl. Acad. Sci. U. S. A. 95, 6163–6168. https://doi.org/10.1073/pnas.95.11.6163.

Zheng, X., Yang, J., Wang, Y., Li, Q., Song, Y., Su, M., Li, J., Zhang, L., Li, Z., Zhou, B., Lin, Y., 2020. RIP1 promotes proliferation through G2/M checkpoint progression and mediates cisplatin-induced apoptosis and necroptosis in human ovarian cancer cells. Acta Pharmacol. Sin. 41, 1223–1233. https://doi.org/10.1038/s41401-019-0340-7.